Progress In Electromagnetics Research M, Vol. 83, 181–190, 2019

Electromagnetic Torque Ripple Minimization of Slotted Doubly-Salient-Permanent-Magnet Generator for Wind Turbine Applications

Lemnouer Bekhouche[1, 2, *], Rachid Saou[1], Cherif Guerroudj[1, 3], A/allah Kouzou[2, 4], and Mohamed El Hadi Zaïm[5]

Abstract—The aim of this work is to reduce the torque ripple of a low-speed/high-torque Doubly Salient Permanent Magnet (DSPM) generator for wind turbine applications. To do this, a combined design and control-based approaches are set up to improve the overall machine performance. The design-based approach helps to develop a form of small stator/rotor teeth combination, focusing on the shapes and dimensions of the teeth that will minimize torque ripple. On the other hand, in the second approach, a control technique is designed. It employs indirect torque control (Torque Sharing Function: TSF), including a PI-controller with gains adjusted continuously for regulating the reference current. The obtained results show that by combining these two approaches, the ripple rate of the electromagnetic torque for the studied DSPM is reduced to a minimum when the teeth shapes are trapezoidal in both the stator and rotor, and the command approach also allows an improvement in the total torque shape, such that the ripple rate decreases by about 96%.

1. INTRODUCTION

The conventional electrical generators, used in wind power systems, are generally coupled to a turbine shaft via a gearbox to get the required speed. These types of speed adaptation system have several disadvantages; for example, they are bulky, costly, and require regular maintenance. To overcome these problems, new structures of variable reluctance machines, operating at low speeds, called slow machines or direct attack machines are proposed [1–10]. One of these structures, named Doubly Salient Permanent Magnet Machine (DSPM), a variable reluctance machine, with a large number of rotor and stator teeth excited by non-rotating permanent magnets housed in the stator yoke, attracts more and more attention [2, 9, 13]. This kind of machines is naturally well suited for low speed because its speed is directly related to the number of rotor teeth. It has no magnets or windings on the rotor, and its stator windings, which are easy to manufacture, do not require any particular technique or professional competence to use. The windings are supported with shorter coil heads which minimizes the quantity of the copper and reduces their resistance. Furthermore, this machine has a simple geometry which reduces its manufacturing cost.

The major disadvantage of this machine is that it engenders high electromagnetic torque ripples that cause vibrations and noises. Several previous works suggesting various approaches for reducing vibrations and acoustic noises in these types of electrical machines have been reported. Most of these

Received 28 May 2019, Accepted 26 July 2019, Scheduled 14 August 2019
* Corresponding author: Lemnouer Bekhouche (blemnouer@gmail.com).
[1] Laboratoire de Génie électrique, Faculté de Technologie, Université de Bejaia, Bejaia 06000, Algeria. [2] Department of Electrical Engineering, Faculty of Science and Technology, Djelfa University, Algeria. [3] Departement d' Électrotechnique, Faculte d' électronique et d'Informatique, USTHB, Bab Ezzouar, Alger 016111, Algeria. [4] Applied Automation and Industrial Diagnostics Laboratory, Faculty of Science and Technology, University of Djelfa, DZ 17000, Algeria. [5] IREENA, Boulevard de Luniversit, Saint-Nazaire 44600, France.

approaches are based on studying the structural topology by considering the machine configuration [11–15] and others on control techniques [16–23] or on compensation techniques [24]. In the present work, two approaches are combined to reduce the generated electromagnetic torque ripple rate. The first approach is used to determine the most appropriate combination of the small stator and rotor teeth in terms of shapes and dimensions. In this approach, three shapes of the rotor and stator teeth are studied: rectangular, circular and trapezoidal. The second approach is based on the application of nonlinear TSF including a PI adaptive gain controller, in which a cubic form of the torque for each phase is imposed in order to obtain a constant total torque. The electrical currents corresponding to the reference torques produced by each phase are determined by the static characteristics of the machine, approximated using the Krigeage interpolation method and controlled by the PI controller with adaptive gains.

2. PRESENTATION AND MODELLING OF DSPM

2.1. DSPM Presentation

The Doubly Salient Permanent Magnet Machine (DSPM), under investigation, is a variable reluctance three-phase machine which has number of rotor and stator teeth $N_r = 64$ and $N_s = 48$, respectively distributed on $N_{dp} = 12$ stator slots (Fig. 1). For its excitation, it has four NdFeB permanent magnets attached to the stator yoke. The stator slots carry the windings of the three phases each consisting of four concentric coils, connected in series so that their magnetic fluxes add up when they are supplied by an electric current. The position of the four magnets of the stator yoke leads to an identical magnetic flux for the three phases which are phase shifted by 120° with respect to each other.

The rotor speed Ω is related to the stator currents frequency of the stator currents f and the number of teeth N_r with following relationship:

$$\Omega = \frac{2\pi f}{N_r} \tag{1}$$

The number of teeth on rotor $N_r = 64$ is fixed in order to obtain a typical electrical frequency of 50 Hz for the nominal speed of 50 rpm.

The main parameters characterizing the machine, shown in Fig. 2, are: the rotor and stator yoke E_r and E_s, the coil height h_b, the slots opening β, the position of A (R_a, β_a) with R_a being the distance

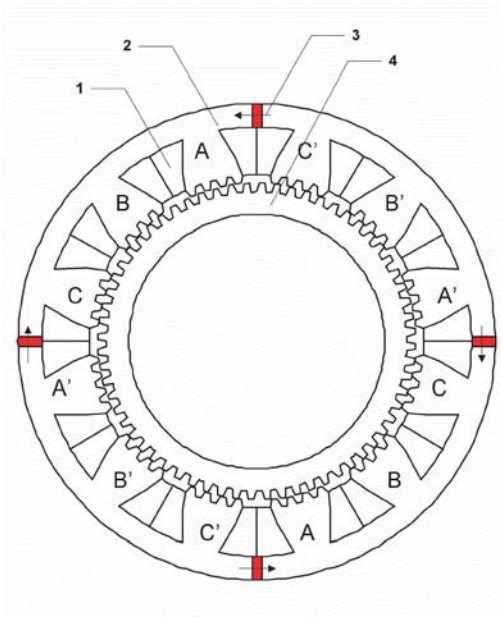

Figure 1. [2] — DSPM reference. 1 — winding of phase A, 2 — stator yoke, 3 — magnet, 4 — rotor yoke.

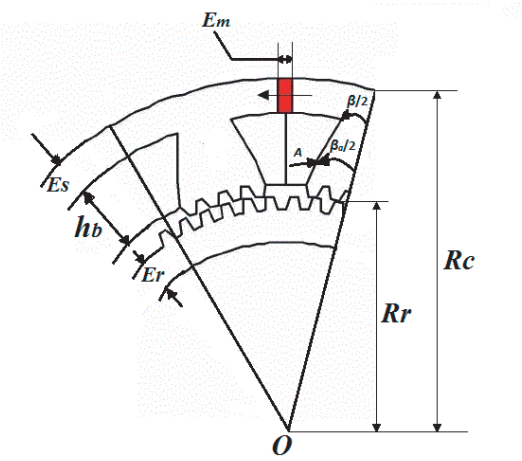

Figure 2. Machine global parameters.

between the A point and machine center O. The stator and rotor teeth parameters are: h_s, α_{s1}, α_{s2} and h_r, α_{r1}, α_{r2}. The magnet thickness is E_m.

2.2. DSPM Modeling

Considering that the three phases are magnetically independent, the voltage V_j at the terminals of a powered phase j is given by:

$$V_j = RIj + \frac{d\phi(\theta, I_j)}{dt} \tag{2}$$

where $j = 1; 2$ and 3 (the three-phases)

I, R, and ϕ represent respectively the current, the resistance of a stator phase, and the magnetic flux per phase. θ represents the rotor position. $\phi(\theta, I_j)$ is composed of flux ϕ_{pm} due to the magnets and flux $\phi_w(\theta, I_j)$ due to the phase current:

$$\phi(\theta, I_j) = L(\theta, I_j)I_j + \phi_{pm} \tag{3}$$

The electromagnetic torque expression is given by:

$$\Gamma_j = \frac{1}{2}I_j^2\frac{dL(\theta, I_j)}{d\theta} + I_j\frac{d\phi_{pm}}{d\theta} = \Gamma_r + \Gamma_{pm} \tag{4}$$

where Γ_{pm} is the hybrid torque due to the interaction between magnet flux and flux due to phase currents, and Γ_r is the reluctance torque.

Since the machine has a high saturation, the inductance varies little according to the rotor position θ; this generates a low reluctance torque value [2, 9].

The hybrid torque Γ_{pm} is then the total torque dominant component and can be produced by applying either a positive current to the phase winding (during flux increases) or a negative current (when the flux decreases). The phases are magnetically independent, such that the total torque is the sum of three torques produced by each phase which is given by

$$\Gamma = \sum_{j=1}^{3}\Gamma_j \tag{5}$$

The machine static characteristics are determined by the finite element method under 2D-FEMM software. The results obtained are presented by networks of curves $\phi = f_1(I, \theta)$ and $\Gamma = f_2(I, \theta)$.

Figure 3 shows the network of magnetic flux characteristics, obtained by the finite element method. These characteristics are highly nonlinear, particularly when approaching the conjunction position. The flux produced by the current is added to that of the permanent magnets, where the machine becomes more saturated when the current is increased. Fig. 3 also shows that the machine flux, produced by the permanent magnet and stator windings inductance, saturates the machine magnetic circuit. Therefore, it is not correct to use the inductance to calculate the flux in the Matlab/Simulink model as stated in [17].

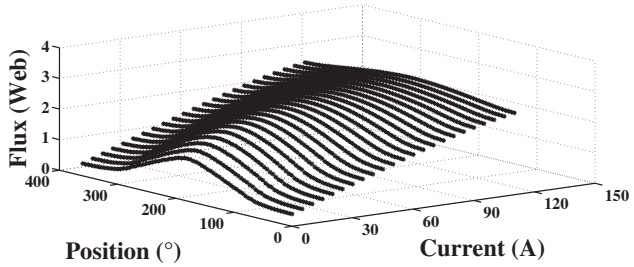

Figure 3. Magnetic flux curve network, obtained by FEM, according to rotor position for different phase currents $\phi = f_1(I, \theta)$.

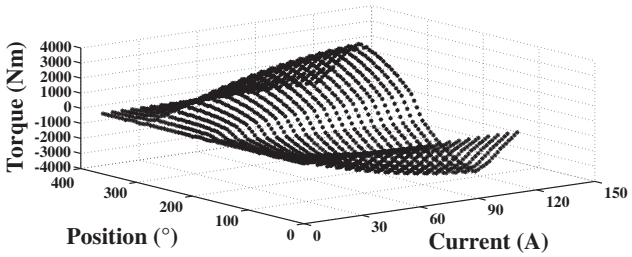

Figure 4. Torque curve network, obtained by FEM, according to rotor position for different phase currents. $\Gamma = f_2(I, \theta)$.

Figure 4 depicts values of the torques obtained for rotor positions between 0° and 180° electrical degrees, corresponding to the generator operation mode, while those obtained between 180° and 360° correspond to the motor operation mode. The distance between the curves decreases as the load current increases. This is essential due to the saturation of the magnetic circuit which also leads to a strong torque ripple.

The DSPM nonlinear model used in Matlab/Simulink, presented in this work, is based on the interpolation of its characteristics. The flux and torque networks (Figs. 3–4) as a function of supply current and the rotor position are determined by 2D-FEMM, then interpolated by Krigeage method with the aids of using Matlab. This interpolation method is better adapted to the DSPM modeling. It makes possible to obtain an interpolation function with derivatives that are not very oscillating in the interpolation domain. The DSPM is characterized by the flux network $\phi = f_1(I, \theta)$ and torque network $\Gamma = f_2(I, \theta)$ as functions of current and the rotor position. Defined by the following general equation:

$$\begin{cases} f(I,\theta) = a_1 + a_2 I + a_3\theta + \sum_{j=1}^{N} \alpha_j g(h) \\ g(h) = h^2 \ln h \ \text{ with } \ h = \sqrt{(I - I_j)^2 + (\theta - \theta_j)^2} \end{cases} \tag{6}$$

Using Equations (2) and (5), we obtain the model of Figs. 5–6.

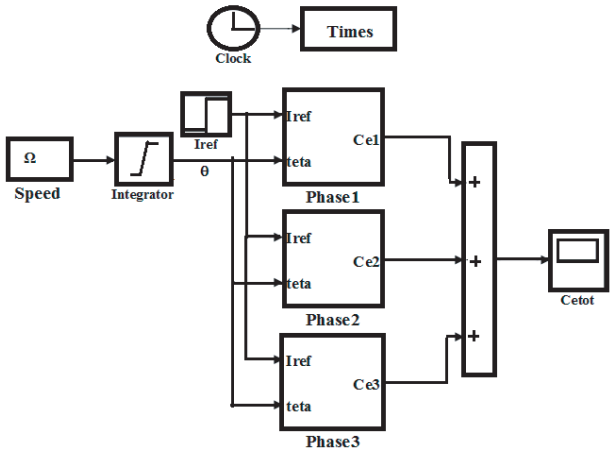

Figure 5. DSPM model. Block of three phases.

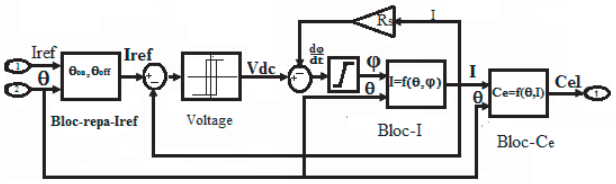

Figure 6. DSPM model. Block phase 1.

In Figs. 5–6 above: Bloc-repa-Iref: allows us to deliver the reference current from the rotor position Bloc-I: permits current interpolation from knowing the flux value calculation and the rotor position knowledge by the Krigeage interpolation. Bloc-Γ allows us to calculate the torque value from the current value knowledge and rotor position.

The model inputs of the DSPM are the voltages. The magnetic flux in the windings is obtained by integrating the difference between the input voltage and the voltage drops across winding resistor. The electric currents in the stator windings are determined by the interpolation function $I = f_3(\phi, \theta)$ using Equation (6). The electromagnetic torques produced by each stator winding are obtained by the nonlinear interpolation function $\Gamma = f_2(I, \theta)$ according to Equation (6) and subsequently summed to give the total torque produced by the machine. Figs. 3–4 are obtained by the interpolation functions (Krigeage) $\phi = f_1(I, \theta)$ and $\Gamma = f_2(I, \theta)$ used in the DSPM model of the Figs. 5–6.

3. RIPPLE RATE CALCULATION

The machine electromagnetic torque is naturally pulsating because of its high magnetic saturation and successive supply phase. The rate of ripple is calculated as following equation

$$\Gamma(\%) = 100 \times \frac{|\Gamma_{\max} - \Gamma_{\min}|}{\Gamma_{\text{average}}} \tag{7}$$

where $\Gamma_{\min}$, $\Gamma_{\max}$, and Γ_{average} are the minimum, maximum, and average electromagnetic torques obtained from the total torque, respectively.

The average torque is given by:

$$\Gamma_{\text{average}} = \frac{qN_r(W'_{\text{aligned}} - W'_{\text{unaligned}})}{2\pi} \tag{8}$$

where q is the number of phases, N_r the number of rotor teeth, and $W'_{\text{aligned}}/W'_{\text{unaligned}}$ are respectively the converted coenergies in the aligned and unaligned positions.

4. ELECTROMAGNETIC TORQUE RIPPLE MINIMIZATION

In order to minimize torque ripples, we first consider the structural approach. This leads to reaching various proper combinations of stator and rotor teeth that will give the minimum torque ripples. The optimal combination will be retained for the second approach, which is based on indirect torque control. It applies the TSF of cubic form, incorporating an adaptive PI-controller which will control the reference current. The main purpose behind it is to improve the machine behavior and thus minimize the ripple rate.

4.1. Structural Approach

It is noted that the machine with teeth plots offers a particular feature of having coils between the stator plots and not in the slot located between the small teeth. Unlike large tooth MRVs, the small teeth shape does not affect the coil surface. This justifies the fact that the small teeth optimization is done for a fixed main structure. The low-speed DSPM main electromagnetic structure optimization

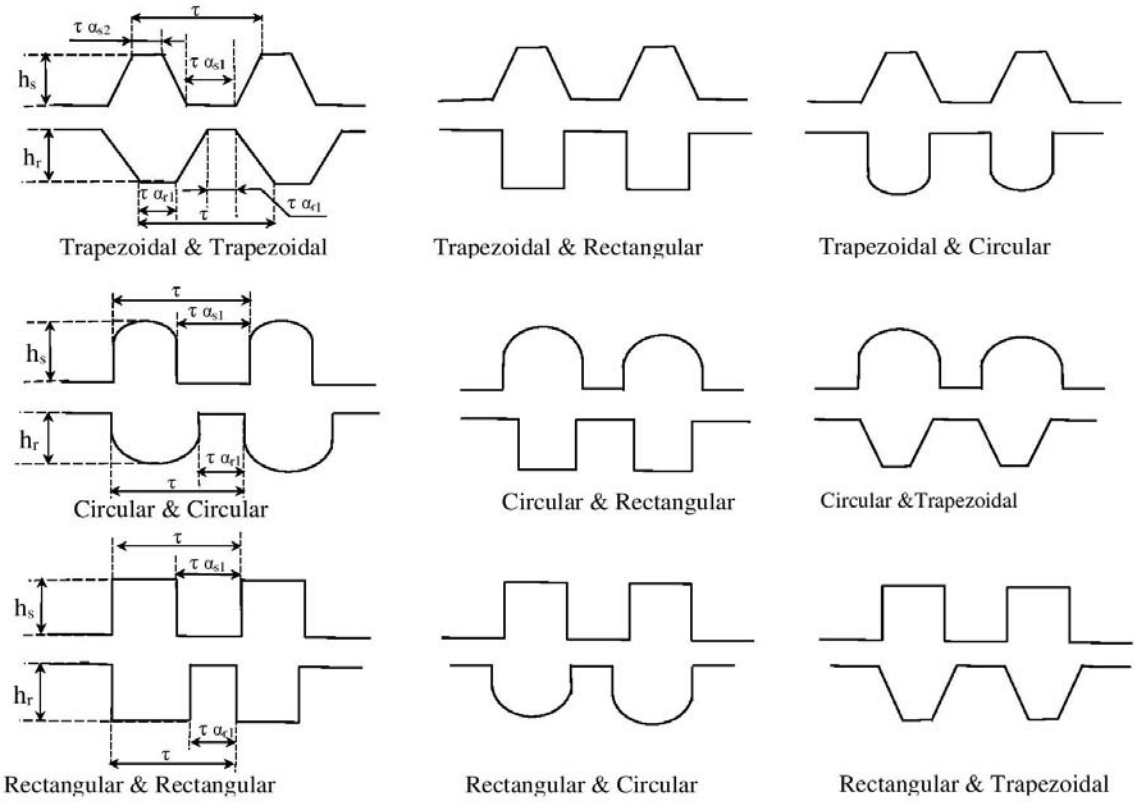

Figure 7. Different shapes and parameters of the studied teeth.

was designed in [3]. The structural approach is based on the study of all the possible combinations between the three forms found in the literature (rectangular RC, circular CR, and trapezoidal TR), and 9 combinations are then possible (see Fig. 7).

4.1.1. Tooth Shape Studies

The main objective of the present work is to study all the possible combinations of the three shapes identified in the literature. They are rectangular, circular and trapezoidal shapes depicted in Fig. 7 to determine the best combination that will minimize the torque ripples of the machine. For each combination, we determine the geometric dimensions of the stator and rotor teeth that maximize the electromagnetic torque of the machine, by keeping the main dimensions of the machine constant. The values of the parameters are obtained for each combination. The optimization method used is based on cyclic relaxation [25] combined with the finite element method. The ripple ratio is calculated by Figs. 7 and 8.

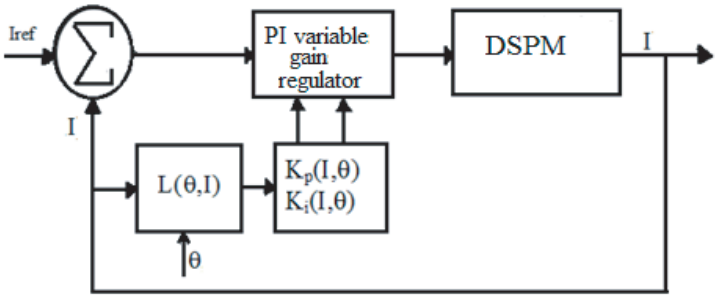

Figure 8. PI variable gain controller.

According to the combinations of the tooth teeth shapes, four to six parameters are to be optimized. The constraints on the optimization variables are given in Table 1. The lower and upper limits of the variables to be optimized, estimated taking into account the physical and electromagnetic constraints, define the search space. Once the parameters have been set for each combination, we will calculate the ripple rates generated by each of them, by 2D-FEM, and retain the structure that will produce the minimum rate.

Table 1. Constraint on the optimization variables.

Parameters	lower limit	Upper limit
α_{r1} and α_{s1}	0.20	0.50
α_{r2} and α_{s2}	0.15	0.5
h_{s1} and h_{r1}	2	15
$\alpha_{j1} + \alpha_{j2} \leq 1$ with $j = r \cdot s$		

4.2. Command Approach

The study in [17, 18, 23] consists in defining the torque appropriate shape for each phase (this technique is called TSF), so that the total torque is constant. The reference currents are directly deduced from nonlinear characteristics of the torque as a function of the current and the position (Fig. 6). The Krigeage interpolation method mentioned above is used to deduce the reference currents. In this article, the reference torque is of the cubic form. The TSF reduces the ripple rate from 107.27% to 21.06%. In order to improve the performance of the TSF, we introduce a reference current regulator whose gains are constantly adapted to the current value in the phase and to the position of the rotor [21].

4.2.1. Variable Gain Controller

The advantage of using the variable gain controller shown in (Fig. 8) is that the system dynamic is under control and do not vary randomly with the variation of the inductance. The design of the controller must be based on the DSPM model as follows:

For each conduction phase one has:

$$V = RI + \frac{d\phi(\theta, I)}{dt} \tag{9}$$

with:

$$\phi(I, \theta) = \phi_{pm} + L(\theta, I)I \tag{10}$$

and:

$$\frac{d\phi(I, \theta)}{dI} = \frac{d\phi_{pm}}{dt} + I\frac{dL(I, \theta)}{dt} + L(I, \theta)\frac{dI}{dt} \tag{11}$$

such that

$$E(I, \theta, \omega) = \frac{d\phi_{pm}(I, \theta)}{d\theta}\frac{d\theta}{dt} + I\frac{dL(I, \theta)}{d\theta}\frac{d\theta}{dt} \tag{12}$$

where $E(I, \theta, \omega)$: The electromotive force. $\frac{d\theta}{dt}$: Rotor rotation speed.

So the voltage equation becomes:

$$V = RI + L(I, \theta)\frac{dI}{dt} + E(I, \theta, \omega) \tag{13}$$

The PI-controller has the form,

$$G(s) = K_p(I, \theta) + \frac{K_i(I, \theta)}{s} \tag{14}$$

The two proportional $K_p(I, \theta)$ and integral gains $K_i(I, \theta)$ are calculated as follows:

$$\begin{cases} K_p(I, \theta) = 2w_n\xi L(I, \theta) \\ K_p(I, \theta) = w_n^2 L(I, \theta) \end{cases} \tag{15}$$

Damping coefficient ξ is set at 0.7 and the bandwidth w_n at 10000 rad/s.

The inductance expression is calculated with:

$$L(I, \theta) = \frac{\partial(\phi(I, \theta))}{\partial I} \tag{16}$$

Flux $\phi(I, \theta)$ is calculated using Krigeage interpolation in Eq. (6).

The variable gain PI-controller is shown in Fig. 8.

5. SIMULATION RESULTS

5.1. Structural Approach Results

5.1.1. Teeth Optimal Parameters of the DSPM

The results obtained by applying the structural approach are illustrated in the following two tables. Table 2 gives the DSPM teeth optimal parameters, optimized by the cyclic relaxation method [25]. The geometry of the rectangular and circular teeth is defined by a single cyclic ratio.

Table 3 gives the ripple rates and maximum torque of different combinations of teeth, and these rates are calculated by Equations (7)–(8). Based on the results given above, it is obvious that the tooth shape has great influence on the value of the torque and also on the torque ripples. The $\text{DSPM}_{\text{TR-CR}}$ machine whose teeth have trapezoidal shape in the stator and circular one in the rotor has the highest ripple rate which is equal to 125.16%, whereas the $\text{DSPM}_{\text{TR-TR}}$ machine, which has trapezoidal teeth in the stator and in the rotor, produces the lowest torque ripples. The ripple rate of 107.27% is obtained by this structure with the highest max torque of 2982.92 Nm. The results also show that $\text{DSPM}_{\text{TR-TR}}$ has better performance than the other DSPMs types studied in this paper. It has the lowest ripple rate and

Table 2. The DSPM teeth parameters optimized.

$DSPM_{Stator\text{-}Rotor}$	TR-TR	TR-RC	TR-CR	RC-TR	RC-RC	RC-CR	CR-TR	CR-CR	CR-RC
h_s	7.450	9.150	6.199	7.000	4.349	4.299	4.000	4.000	4.000
h_r	10.00	7.050	4.099	8.700	6.299	4.000	8.100	4.800	0.050
α_{s1}	0.195	0.200	0.165	0.280	0.250	0.260	0.300	0.270	0.300
α_{s2}	0.270	0.255	0.285	–	–	–	–	–	–
α_{r1}	0.325	0.330	0.365	0.300	0.345	0.275	0.250	0.375	0.300
α_{r2}	0.265	–	–	0.405	–	–	0.300	–	–

Table 3. The DSPM torque ripple and max torque.

$DSPM_{Stator\text{-}Rotor}$	TR-TR	TR-RC	TR-CR	RC-TR	RC-RC	RC-CR	CR-TR	CR-CR	CR-RC
Ripple torque (%)	107.27	110.91	112.80	113.61	114.83	120.45	120.60	120.73	125.16
Max torque (Nm)	2982.92	2578.03	2888.62	2628.57	2655.13	2451.89	2877.75	2508.09	2892.14

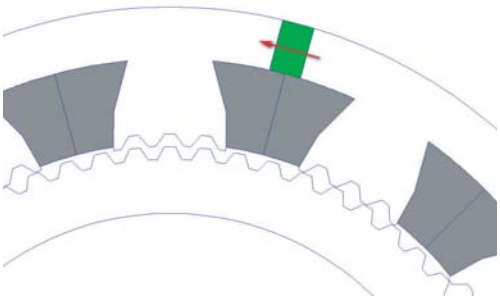

Figure 9. The teeth geometry of the optimal DSPM.

the highest torque. This is because the variation of the reluctance is greater in this case, and magnetic flux leakage around the teeth is reduced resulting in a substantial increase in the electromagnetic torque. The latter structure, whose shape and dimensions of teeth are shown in Fig. 9, will be used for the second approach.

5.2. Command Approach Results

The simulation result of the applied control, depicted in Fig. 10, exhibits a good performance that leads to an improvement in the total torque delivered by the machine. The electromagnetic torque of each phase follows the trajectory (cubic shape) that is imposed by the nonlinear control (the TSF with a variable gain PI-controller). This produces a constant total torque, which results in a reduction in torque ripples. A reduction of 96.79% is obtained in the ripple rate which decreases from 107.27% to 10.48%. The current flowing in the DSPM windings follows the reference current, under the effect of the PI variable-gain controller as illustrated in Fig. 11. The two peaks at 50 degrees and 140 degrees correspond to the positions of the teeth close to the intermediate position (between aligned and unaligned ones) which require a high current to produce a large torque.

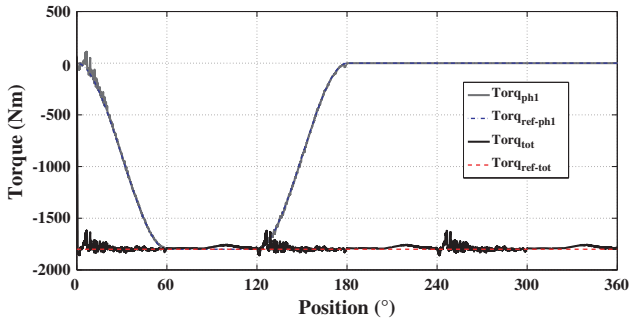

Figure 10. Total torque variation (Cubic shape).

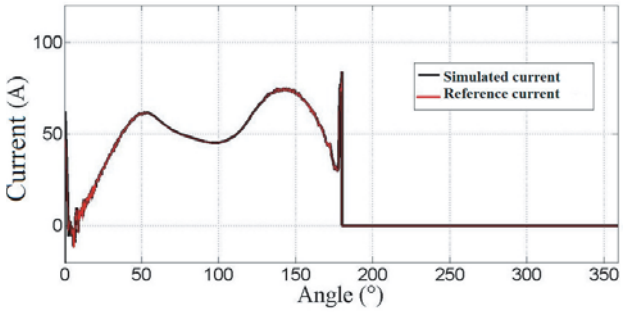

Figure 11. Current variation for a Cubic form of torque.

6. CONCLUSION

In order to reduce the electromagnetic torque ripple of the low speed variable reluctance generator (DSPM), two approaches are proposed in this paper. The first approach is based on a DSPM structure, namely the combination of small rotor and stator teeth in terms of shapes and geometric dimensions. The shapes of the small teeth have a great influence on the torque ripple. When the stator teeth are trapezoidal and the rotor teeth circular, the resulting torque is the most corrugated. On the other hand, when the teeth are trapezoidal in both the stator and rotor, the ripple rate of the electromagnetic torque is reduced to a minimum. Concerning the second approach, it is based on the control that allows us to impose appropriate forms of the reference torque for each phase. This would give a constant total torque (TSF with variable gain reference current controller). This command allows an improvement in the total torque shape, such that the ripple rate is decreased from 107.27% to 10.48%. Finally, based on the obtained results, it is found that the proposed combined approach is a promising solution for the electric machines used in wind power generation systems to overcome the main disadvantages found in conventionally used systems. In perspective of this work, it will be for us to implement the command TSF on a DSPM prototype integrated into an autonomous wind energy.

REFERENCES

1. Moreau, L., M. Machmoum, and M. E. Zaïm, "Design of low-speed slotted switched reluctance machine for wind energy applications," *Ele. Pow. Comp. and Sys.*, Vol. 34, No. 10, 1139–1156, 2006.
2. Saou, R., M. E. Zaïm, and K. Alitouche, "Optimal designs and comparison of the doubly salient permanent magnet machine and flux-reversal machine in low-speed applications," *Power Components Syst.*, Vol. 36, No. 9, 914–931, 2008.
3. Saou, R., M. E. Zaïm, and K. Alitouche, "Modelling and design of a low speed flux reversal machine," *J. Electr. Syst. 2009*, Vol. 36, No. 9, 18–23, 2009.
4. Tarimer, I. and Â. Sakar, "Effects of structural design of pole arc offset in a salient pole generator to obtaining sinusoidal voltages with the least harmonics," *Przeglad Elektrotechniczny*, Vol. 2010, No. 11a, 367–372, 2010.
5. Tarimer, I. and E. O. Yuzer, "Designing of a permanent magnet and directly driven synchronous generator for low speed turbines," *Ele. and Electrical Eng.*, Vol. 6, No. 112, 15–18, 2011.
6. Rupar, U., F. Lahajnar, and P. Zajec, "Iterative-learning-based torque-ripple compensation in a transverse flux motor," *IET Cont. Theo. App.*, Vol. 6, No. 3, 341–348, 2012.
7. Shi, U. C., D. C. Yon, C. W. Byung, D. K. Hong, and J. Y. Lee, "Design considerations and validation of permanent magnet vernier machine with consequent pole rotor for low speed servo applications," *J. Electr. Eng. Technol.*, Vol. 8, No. 5, 1146–1151, 2013.

8. Topaloglu, I., C. Ocak, and I. Tarimer, "A case study of getting performance characteristics of a salient pole synchronous hydrogenerators," *Elektronika ir Elektrotechnika*, Vol. 97, No. 1, 57–61, 2015.
9. Guerroudj, C., R. Saou, A. Boulayoune, E. M. Zaïm, and L. Moreau, "Performance analysis of Vernier slotted doubly salient permanent magnet generator for wind power," *Int. J. Hyd. Ene.*, Vol. 42, No. 13, 8744–8755, Mar. 30, 2017.
10. Ocak, C., D. Uygun, and I. Tarimer, "FEM based multi-criterion design and implementation of a PM synchronous wind generator by fully coupled co-simulation," *Adv. in Ele. and Comp. Eng.*, Vol. 18, 37–42, 2018.
11. Soong, W. L. and N. Ertugrul, "Field-weakening performance of interior permanent-magnet motors," *IEEE Tran. on Indu. App.*, Vol. 38, No. 5, 1251–1258, 2002.
12. Sahin, C., A. E. Amac, M. Karacor, and A. Emadi, "Reducing torque ripple of switched reluctance machines by relocation of rotor moulding clinches," *IET Ele. Pow. Appl.*, Vol. 6, No. 9, 753–760, 2012.
13. Guerroudj, C., R. Saou, F. Charpentier, and A. Boulayoune, "Optimal design of a novel doubly salient permanent magnet motors for high power ship propulsion," *2018 XIII ICEM*, 2556–2562, IEEE, Alexandroupoli, 2018.
14. Jing, L. and J. Cheng, "Research on torque ripple optimization of switched reluctance motor based on finite element method," *Progress In Electromagnetics Research M*, Vol. 74, 115–123, 2018.
15. Massimo, B., P. Tomas, and F. Ivano, "Low-torque ripple design of a ferrite-assisted synchronous reluctance motor," *IET Ele. Pow. App. Spec.*, Vol. 10, No. 5, 319–329, 2016
16. Ketabi, A., A. Yadghar, and M. J. Navardi, "Torque and ripple improving of a SR motor using robust particle swarm optimization of drive current and dimension," *Progress In Electromagnetics Research M*, Vol. 45, 195–207, 2016.
17. Moreau, L., M. Machmoum, and M. E. Zaim, "Control and minimization of torque ripple in switched reluctance generator," *Eur. Conf. Power Electron. Appl.*, 1–8, Dresden, 2005.
18. Xue, X. D., K. W. E. Cheng, and S. L. Ho, "A control scheme of torque ripple minimization for SRM drives based on flux linkage controller and torque sharing function," *2nd Int. Conf. Power Electron. Syst. Appl. ICPESA*, 79–84, Hong Kong, 2006.
19. Gobbi, R. and K. Ramar, "Optimisation techniques for a hysteresis current controller to minimise torque ripple in switched reluctance motors," *IET Ele. Pow. App.*, Vol. 3, No. 5, 453–460, 2009.
20. Xia, Y. Y., J. E. Fletcher, S. J. Finney, K. H. Ahmed, and B. W. Williams, "Torque ripple analysis and reduction for wind energy conversion systems using uncontrolled rectifier and boost converter," *IET Ren. Pow. Gen.*, Vol. 5, No. 5, 377–386, 2011.
21. Hannoun, H., M. Hilairet, and C. Marchand, "High performance current control of a switched reluctance machine based on a gain-scheduling PI controller," *Control Eng. Pract.*, Vol. 19, No. 11, 1377–1386, 2011.
22. Korkmaz, F., I. Topaloğlu, H. Mamur, M. Ari, and I. Tarimer, "Reduction of torque ripple in induction motor by artificial neural multinetworks," *Turk. J. Elec. Eng. & Comp. Sci.*, Vol. 24, 3492–3502, 2016.
23. Milad, D., M. S. N. Seyed, and W. A. Jin, "Torque ripple minimization of switched reluctance motor using modified torque sharing function," *2013 21st Iran. Conf. Electr. Eng. ICEE 2013*, 1–6, Mashhad, 2013.
24. Lange, T., B. Kerdsup, C. Weiss, and R. W. De Doncker, "Torque ripple reduction in reluctance synchronous machines using an asymmetric rotor structure," *7th IET Int. Conf. PEMD 2014*, 1–5, Manchester, 2014.
25. Tahi, S., R. Ibtiouen, and S. Mekhtoub, "Performance optimization of synchronou reluctance machines with two rotor structures," *ICEM 2014*, 250–255, Berlin, 2014.